Monitored indentation for the detection of inclusions in elastomer material

Anne-sophie Caro, Sarah Iaquinta, Sarah Chhean, Léa Guérandelle, Yohann Mewa Singh, Romain Léger, Jonathan Barés, Arnaud Regazzi, Stéphane Corn, Patrick Ienny

Monitored indentation for the detection of inclusions in elastomer material.

Anne-Sophie Caro[1], Sarah Iaquinta[1], Sarah Chhean[1], Léa Guérandelle[1], Yohann Mewa Singh[1], Romain Léger[1], Jonathan Barés[2], Arnaud Regazzi[1], Stéphane Corn[1], Patrick Ienny[1]*

Affiliation 1

A.S Caro, S. Chhean, S. Corn, L. Guérandelle, S. Iaquinta, P. Ienny, R. Léger, Y. Mewa Singh, A. Regazzi

LMGC, IMT Mines Ales, Univ Montpellier, CNRS, Ales, France

C2MA, IMT Mines Alès, 6 avenue de Clavières, 30319 Alès Cedex, France

Affiliation 2

LMGC, Univ Montpellier, CNRS, Montpellier, France

Campus Saint Priest, 860 rue Saint Priest, 34090 Montpellier

ORCID ids and emails of the authors

A.S Caro	0000-0001-7743-1915	Anne-sophie.caro@mines-ales.fr
S. Chhean		Sarah.chhean@mines-ales.org
S. Corn	0000-0002-9819-0425	Stephane.corn@mines-ales.fr
J. Barés	0000-0002-7345-0390	Jonathan.bares@umontpellier.fr
L. Guérandelle		Lea.guerandelle@mines-ales.org
*S. Iaquinta	0000-0002-6756-5992	Sarah.iaquinta@mines-ales.fr
P. Ienny	0000-0002-7173-5210	Patrick.ienny@mines-ales.fr
R. Léger	0000-0003-1849-2341	Romain.leger@mines-ales.fr
Y. Mewa Singh		Yohann.mewa-singh@mines-ales.org
A. Regazzi	0000-0002-6070-2878	Arnaud.regazzi@mines-ales.fr

Keywords: hyper-viscoelasticity, adhesion, stereo-image correlation, indentation

Abstract

The detection of inclusions in soft material is of great interest, especially in the medical field. Traditionally, a biopsy exam is performed after palpation, when necessary. In the present work, a potentially quantitative method, via monitored indentation, is used to mimic palpation. This method consists in investigating the relaxation and stress-free relaxation responses to an indentation test performed on a silicone block with an inclusion. The aim of the study is to evaluate how a difference in position, size and adhesion of the inclusion can influence the response of the samples to monitored indentation. A finite element model is constructed to conduct comparative studies. The hyper-viscoelastic parameters of the silicone have been identified experimentally. Results from the simulations showed that the indicators measured

during monitored indentation, especially during the stress-free relaxation phase, are sensitive to adhesive inclusions, while they provide little information regarding their non-adhesive counterparts. Depths and sizes for which adhesive inclusions are more likely to be detected have been identified. These results are encouraging but are conducted on polymer material and a rigid inclusion; nevertheless, they suggest that the non-destructive measure of the stress-free relaxation response of a tissue may help practicians to quantitatively characterize the nature of a nodule.

1. Introduction

The quantitative measurements of the mechanical properties of soft tissues are fundamental in various fields of applications, e.g. diagnosis, reconstruction and modeling (Haddad et al. 2020; Pierrat et al. 2018; B. Rao, and Pandya 2019). Manual palpation techniques are, for instance, widely used for the detection of superficial nodules, whose malignancy can, in some extent, sensitively be determined by the practicians. This technique allows decision for further quantitative analyses, e.g. medical imaging techniques (Kuhl, 2000). Unfortunately, many tumors cannot be detected manually, either because they are too small or too deep (McDonald et al., 2004).

Instrumented indentation techniques are commonly used to mimic palpation as they enable to control the boundary conditions of the measure, which minimizes the variability due to the operator who conducts the measure (Bendtsen, Jensen, Jensen, & Olesen, 1995). However, most of the existing equipment focus on the analysis of the (i) indentation step, while very little work is devoted to the response of the tissue during (ii) relaxation and (iii) stress-free relaxation. Phase (i) and (ii) respectively consist in investigating the behavior of the material when the indenter is maintained in the same in-depth position and once the indenter is instantaneously pulled out. It may therefore be possible to obtain additional indications concerning the response of the material, whose change could be due to the presence of a nodule and potentially to the nature of its interface with the environment (cohesive or adhesive). The objective of this work is to determine whether instrumented indentation, along with the relaxation and stress-free relaxation phases, can provide sufficient information to identify and characterize the nature of the adhesion between the nodule and the surrounding medium. The effect of the size and position of the nodule on the testing is also investigated. A preliminary study on a surrogate material is proposed. Silicone samples have been chosen since some silicone grades are actually already used as phantoms for certain soft tissues (Sparks et al. 2015). Moreover, the homogeneity of this material as well as its isotropy greatly simplify the interpretation of indentation tests (Kalyanam, Toohey, and Insana 2021).

In this article, the response to the monitored indentation (MI) of a silicone sample is investigated experimentally. Then, steel beads with (resp. without) surface treatments are included into the silicone sample to mimic the presence of tumor with extreme interfacial properties. MI is then performed in both cases to observe the alteration of the response of the material. A finite element model has subsequently been built in order to investigate the influence of the size and position of the inclusion on the measure.

2. Materials and Methods

2.1. Sample preparation and devices

The silicone used is the Ecoflex™ 00-10 obtained from Smooth-On, Inc (Easton, Pennsylvania). Ecoflex™ is a platinum-catalyzed silicone mixed by equal parts of liquid ingredients. The samples were produced by mixing two liquid parts with 1:1 ratio for 3 minutes and then pouring the mixture into molds. Cross-linking (platinum catalyst) was obtained after 4 hours at room temperature and 1 hour at 110 °C. Both cylindrical and rectangular samples have been made. Glass container of 100 mm in diameter and 60 mm in height were used to make cylindrical samples of 36 mm in height. In this case, a polar frame $(\boldsymbol{e}_r, \boldsymbol{e}_\theta, \boldsymbol{e}_z)$ is adopted (cf. **Figure 1**a). Rectangular molds covered by a layer of poly(tetrafluoroethylene) (PTFE) enabled to produce strips (length 35 mm, width 3 mm, thickness 1 mm). In this case, a cartesian frame $(\boldsymbol{x}, \boldsymbol{y}, \boldsymbol{z})$ is adopted (cf. Figure *1*d).

Figure 1: Cylindrical silicone sample (a), steel beads (b), steel beads inside the silicone to simulate nodules (c) and stripped silicone sample (d).

Steel beads of 12 mm in diameter were used. Steel has been chosen for sake of simplicity, as the beads would not deform. The latter were washed three times with ethanol under sonication (5 minutes) to remove any organic pollutants and mineral microparticles. After this step of purification, a strong adhesion between the beads and the polymer could be observed. To avoid adhesion, a PTFE-based aerosol is used. In this case, there is a complete decohesion between silicone matrix and nodules. A flax string was glued to each inclusion to prevent it from sinking in the bottom of the mould before full curing. This way, their position was controlled in the silicone block. After cross-linking, the thread was cut as close as possible from the top surface of the silicone. The inclusions have initially been laid at a position $z = 1.8$ cm in the center of the sample, but the difference in density between silicone and steel yielded a displacement of the inclusions. The positions of the inclusions were therefore determined after the testings, by cutting the silicone sample in two parts. Three samples were made: (i) raw silicone without inclusion, (ii) silicone with adhesive steel inclusion (namely Silicone Steel A) and (iii) silicone with non-adhesive steel inclusion (namely Silicone Steel NA). These samples respectively mimic (i) a breast tissue without nodule, (ii) one with an adhesive tumor and another one (iii) with a non-adhesive tumor. A summary of the manufactured samples, along with their denomination and the position of the inclusion, is presented in **Table 1.**

Table 1: Silicone samples denomination along with the position of the inclusions into the silicone sample.

Denomination	Description	Position of the center of the inclusion
Silicone	Silicone sample without inclusion	Not relevant
Silicone Steel A	Silicone sample with an Adhesive inclusion	$r = 0, z = 2.3$ cm
Silicone Steel NA	Silicone sample with a Non-Adhesive inclusion	$r = 0, z = 1.9$ cm

A home-made device was developed to perform MI testing. It is made of a spherical indenter (10 mm in diameter) tied to a rigid rod, sliding in a tubular frame. When pushed, this rod stretches two springs, and this stretched position can be maintained by electromagnets. Hence, there are two positions for the indenter: (i) an extended position for the indentation/relaxation phases (**Figure 2**a), during which the electromagnets are activated and the springs compressed, and (ii) a folded position (Figure *2*b), for the stress-free relaxation phase during which the electromagnets are deactivated, the springs extended and the indenter in its upper position. This device is fixed to the load cell on the crosshead so that the indenter displacement is known, and the reaction force is measured. The compliance of this device was estimated around 0.028 mm/N. The surface of the sample is covered with talc to minimize friction between the indenter and the silicone. The indentation depth is set to 5 mm, which is reached with a displacement speed of 100 mm/min.
The position is maintained for 30 s (relaxation phase), after which the indenter is removed, leaving room for the observation of the surface displacement (stress-free relaxation phase) for 30 s. As soon as the indenter is removed, two cameras (Basler acA3088-57um) with a 50 mm lens record the evolution of the previously black-pattern-painted surface of the sample from two different angles. Image sequences are recorded with a 55 Hz frequency and a 0.1 mm per pixel scale factor. The three-dimensional (3D) displacements are computed using 3D Digital Image Correlation (DIC) processing (®VIC 3D software). The out-of-plane displacement of the points *A* and *B* on the surface of the silicone and under the indenter are specifically extracted. During this instrumented test, two variables are recorded: the axial load (F) during the indentation and relaxation phases and the out-of-plane displacement (w) of the point *A*.

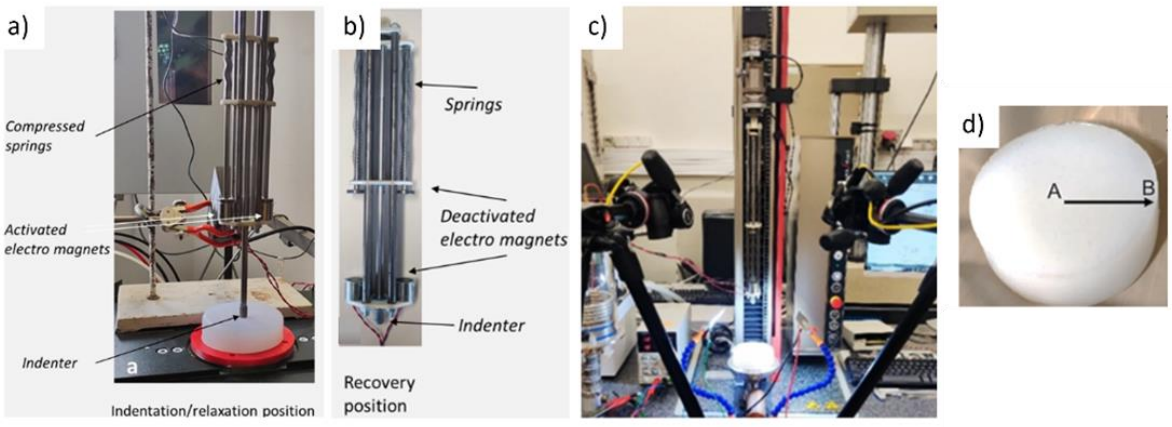

Figure 2: Indentation device in the indentation or relaxation positions (a) and in the stress-free relaxation position (b). Representation of the optical setup for the measure of the surface displacement during the relaxation phase (c), illustration of the position (b). Representation of

the optical setup for the measure of the surface displacement during the relaxation phase (c), illustration of the position of points A and B (d)

2.2. Numerical model

A model of the indentation of the silicone sample is built in order to investigate the influence of the configuration of the nodule (e.g. its size or position) on the variables measured during the MI testing, while limiting time and resources expanses. To construct this model, it is necessary to identify the parameters of the behavior law of the investigated material. The latter is first presented via a phenomenological model in Section 2.1.1. The values of the involved parameters are then identified in Section 2.1.2.

2.2.1. Phenomenological model of the behavior of the silicone sample

Ecoflex™ silicone materials exhibit an isotropic incompressible hyper-viscoelastic behavior (Liao et al. 2021; Liao, Hossain, and Yao 2020). The constitutive behavior of such material is usually derived from the strain energy density W, which can be written in terms of the strain gradient $\boldsymbol{F}$ through the right Cauchy-Green deformation tensor $\boldsymbol{C}$, defined as $\boldsymbol{C} = \boldsymbol{F}^T\boldsymbol{F}$. The strain energy is decomposed into three parts, related to: (i) the hydrostatic loads applied to the material, W_{vol}, (ii) the hyperelasticity of the material, W_H, and (iii) its viscosity, W_μ. In the case of incompressible materials, W_{vol} vanishes, yielding $W = W_H + W_\mu$. In this work, the Yeoh's incompressible hyperelastic behavior law (Yeoh 1990) is used. Hence, $W_H = c_1(I_1 - 3) + c_2(I_1 - 3)^2 + c_3(I_1 - 3)^3$, in which I_1 is the first invariant, defined as $I_1 = \mathrm{tr}(\boldsymbol{F}^T\boldsymbol{F})$ and (c_1, c_2, c_3) are material parameters to be determined. The strain energy density due to the viscosity of the material follows a Maxwell model with N elements, yielding $W_\mu = \sum_{m=1}^{N} \psi_m$, where $\psi_m, m \in \{1, \dots, N\}$, is the strain energy density related to each m Maxwell element, which are defined via a relaxation time τ_m, an energy factor β_m and a non-equilibrium stress tensor $\boldsymbol{Q}_m$, defined as $\boldsymbol{Q}_m = \partial\psi_m/\partial\boldsymbol{C}$. The number of elements N of the Maxwell model depends on the solicitation that is applied to the material. For instance, a uniaxial stress relaxation is modeled with $N = 2$ elements. The aforementioned variables verify the following differential equation:

$$\tau_m \dot{\boldsymbol{Q}}_m + \boldsymbol{Q}_m = \tau_m \beta_m \dot{\boldsymbol{S}}_H, \quad (1)$$

where the overdot denotes the derivative with respect to time and $\boldsymbol{S}_H$ is the hyperelastic component of the second Piola-Kirchoff stress tensor, defined as follows:

$$\boldsymbol{S} = \underbrace{2\frac{\partial W_H}{\partial \boldsymbol{C}}}_{\boldsymbol{S}_H} + \underbrace{2\frac{\partial W_\mu}{\partial \boldsymbol{C}}}_{\boldsymbol{S}_\mu}, \quad (2)$$

2.2.1 Identification of the material parameters

The objective of this section is to identify the material parameters $(c_1, c_2, c_3), (\tau_m, \beta_m),\ m \in \{1, \dots, N\}$, to properly describe the behavior of the silicone sample during indentation, relaxation and stress-free relaxation. The nature of these solicitations being complex, a large amount of material parameters is to be determined. This will be done using a Levenberg-Marquart optimization of the correlation between the numerical and experimental results. The expected non-unicity of the solution of the optimization makes necessary the use of a pertinent initial guess. Uniaxial stress relaxation testings, from which the parameter identification is easier than on the MI test has analytical modelling can be performed, have therefore been conducted. The value of the aforementioned parameters will subsequently be used as initial solution for the optimization.

Determination of initial solutions via uniaxial stress relaxation testing

Presentation of the instrumented uniaxial device

Raw silicone was first studied using a homogeneous tensile testing machine, instrumented with one camera to perform DIC and to consider the possible jaws slippage (Caro-Bretelle, Ienny, and Leger 2013). Tests were conducted on the strip silicone samples, using a Zwick TH010 universal testing machine, controlled with the TestXpert II® software, which enabled the synchronized recording of time, load (F) and displacement. Uniaxial tension in the $\boldsymbol{x}$ direction was applied at a crosshead speed of 37 mm/min until a displacement of 23 mm was reached in $t_1 = 37$ s, corresponding to a longitudinal elongation $\lambda_{xx} = 1.67$. The strain-stress curve resulting from this testing is illustrated in **Figure 3.**

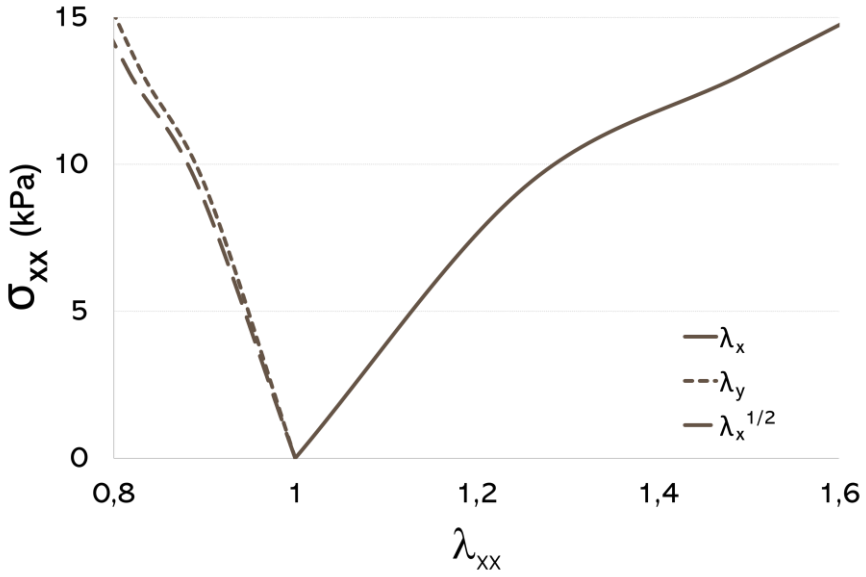

Figure 3: Stress - elongation curves for a uniaxial tensile test of the silicone.

The loading process was then followed by a relaxation phase of 60 s, ending at time $t_2 = t_1 + 60\ s$. During this test, the homogeneous nominal stress $\boldsymbol{\sigma} = \sigma_{xx}\boldsymbol{x} \otimes \boldsymbol{x}$ and the deformation gradient tensor $\boldsymbol{F} = \lambda_{xx}\,\boldsymbol{e_x} \otimes \boldsymbol{e_x} + \lambda_{yy}\,\boldsymbol{e_y} \otimes \boldsymbol{e_y} + \lambda_{zz}\,\boldsymbol{z} \otimes \boldsymbol{z} + \lambda_{xy}\,\boldsymbol{x} \otimes \boldsymbol{y}$ were followed. Note that $\lambda_{i,j}, (i,j) \in \{x,y,z\}^2$, stands for the elongation of the material in different directions. The hypothesis of transverse isotropy ($\lambda_{yy} = \lambda_{zz}$) enabled to follow $\boldsymbol{F}$ with a single camera.

Direct computation

The stress-strain curves given in Figure *3* confirmed the approximation $\lambda_{yy} = {\lambda_{xx}}^{-1/2}$. Hence, during the tension phase ($0 \le t \le t_1$), the strain gradient can be written in terms of the axial elongation λ_{xx}, whose notation is simplified to λ, as $\boldsymbol{F} = \mathrm{diag}\left(\lambda, \lambda^{-1/2}, \lambda^{-1/2}\right)$. In this case, $\boldsymbol{S}_H = \mathrm{diag}(S_H, 0,0)$ and $\boldsymbol{Q}_m = \mathrm{diag}(Q_m, 0,0)$ (Steinmann, Mokarram, and Possart 2012), in which:

$$S_H(t) = 2\left(c_1 + 2\,c_2\left(\lambda(t)^2 + 2/\lambda(t)\right) + 3\,c_3\left(\lambda(t)^2 + 2/\lambda(t)\right)^2\right)(1-\lambda(t)^{-3}). \qquad (3)$$

Using Equation (1), Equation (3) becomes:

$$S(t)=2\left(c_1+2\,c_2\left(\lambda(t)^2+{}^2/_{\lambda(t)}\right)+3\,c_3\left(\lambda(t)^2+{}^2/_{\lambda(t)}\right)^2\right)(1-\lambda(t)^{-3})+\sum_{m=1}^{N}Q_m(t). \quad (4)$$

During the relaxation phase ($t_1 \le t \le t_2$), the load evolved while λ was maintained to 1.67, i.e. $\dot{\lambda}(t) = 0$, yielding $\dot{S}_H(t) = 0$. Equation (1) becomes:

$$\tau_m \dot{Q}_m(t) + Q_m(t) = 0. \quad (5)$$

The solution of this equation is $Q_m(t) = k_m e^{-t/\tau_m}$, where k_m is a constant to be determined. Finally, Equation (4) becomes Equation (6).

$$S(t) = 2\left(c_1+2\,c_2\left(\lambda(t)^2+{}^2/_{\lambda(t)}\right)+3\,c_3\left(\lambda(t)^2+{}^2/_{\lambda(t)}\right)^2\right)(1-\lambda(t)^{-3})+\sum_{m=1}^{N}k_m e^{-t/\tau_m} \quad (6)$$

This equation simplifies into:

$$S(t) = S_H(t_1) \pm \sum_{m=1}^{N} k_m e^{-t/\tau_m} \quad (7)$$

The relaxation times $\tau_{m=1,..,N}$ can therefore be identified from experiments, independently of c_1, c_2, c_3 and $\beta_{m=1,..,N}$. The values of $\tau_{m=1,..,N}$ are determined in the following section. In order to compare experimental data to the model, the first Piola Kirchoff stress, denoted as Π(t) and defined as $\Pi(t) = \boldsymbol{F}\, S(t)$, is introduced.

Identification of the relaxation times of the silicone after tension

The simple evolution of the load $\boldsymbol{F}$ in this case enables a direct evaluation of the relaxation times from the experimental results following the procedure described in the previous section. The relaxation part of the nominal axial stress versus time curve is used. The experimental data is represented in **Figure 4**, along with the 2-element Maxwell model, whose relaxation times τ_1 and τ_2 have respectively been set to 8.4 s and 16 s to fit the experimental relaxion curve. These values will be used as initial guesses for the optimization of the material parameters during the MI testing.

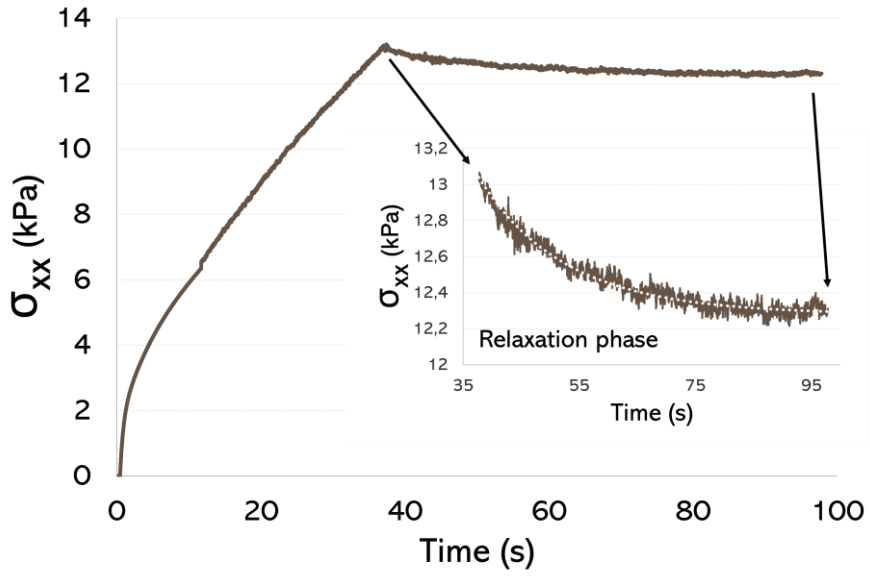

Figure 4: Axial stress versus time for a stress relaxation test. The solid line shows the experimental measurement while the white dotted line shows the modeled result. The inset is a zoom on the second part of the curve.

Values for $\tau_{m=1,2}$ have been determined in the case of a uniaxial stress relaxation test. These values will be used as initial guesses for the optimization of the material parameters in the model of MI, which is presented in the following section.

Structural indentation test: numerical modeling

The MI test was numerically modeled with the finite element analysis method, using the COMSOL Multiphysics® software. The objective was to find a set of mechanical parameters $(c_1, c_2, c_3), (\tau_m, \beta_m),\ m \in \{1, \dots, N\}$, that enabled both the correspondence between numerical and experimental axial load during the indentation/relaxation phases and the numerical and experimental displacement of the surface central point *A* of the raw silicone during stress-free relaxation. The procedure, the so-called FEMU method, is fully described in a previous paper (Avril et al., 2008). Once the parameters for the raw silicone have been determined, a final validation of the correlation between the numerical and experimental results is performed on the silicone samples containing adhesive and decohesive inclusions. The numerical model is presented and the parameters of the constitutive law of the silicone are subsequently identified in the following sections0. A validation is then performed.

Presentation of the model

The geometry of the sample is modeled in two dimensions with an axisymmetric assumption, similarly to existing indentation studies (Zheng, Crosby, & Cai, 2017; Alliliche, Renaud, Cros, & Feng, 2023). This simplification for the numerical model can be made thank to the homogeneity and isotropy of the silicone. The numerical indentation tests are reproduced in the same conditions as the experimental tensile tests, i.e. same imposed displacement, deformation speed and relaxation and stress-free relaxation durations. Unilateral contact without friction and perfect sliding contact between the indenter and the silicone sample is assumed. Vertical displacements (z axis) of the bottom surface of the sample are disabled. The geometries, along with the boundary conditions and mesh used to model the samples with and without inclusion, are illustrated in **Figure 5**. The number of elements and the refinement strategy of the mesh are set after the results of a mesh refinement study. In the case of adhesive inclusions, a perfect contact is assumed between the surface of the inclusions and the surrounding silicone. In the case of non-adhesive inclusions, a frictionless unilateral contact is considered.

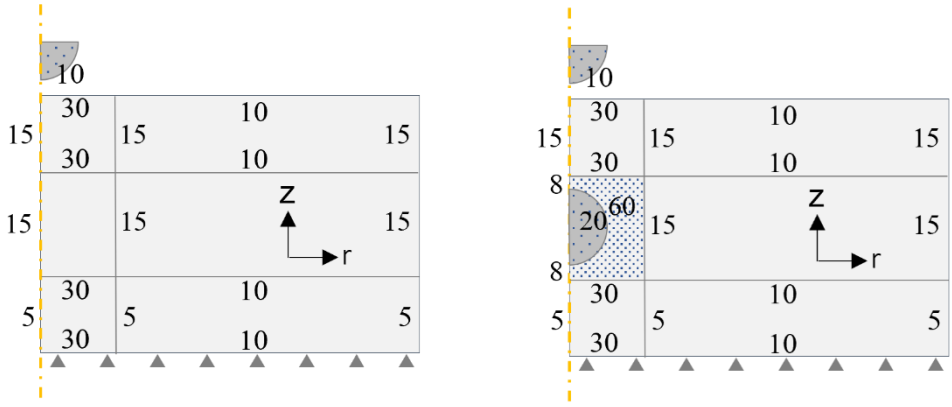

Figure 5: Illustration of the geometry, boundary conditions and meshes used to model the indentation of raw silicone (left) and silicone with inclusion (right). The numbers in the illustrations stand for the number of elements used per edge. The light grey regions are meshed

with structured tetraedric elements using linear interpolation and no reduced integration, while the dotted parts are meshed with free tetraedric elements.

The steel indenter in modeled as a non-deformable body and the steel inclusions are considered to follow an elastic behavior with a Young's modulus $E = 170$ GPa and a Poisson's ratio $\nu = 0.28$.

Identification of the constitutive parameters of the raw silicone

MI tests are triaxial structural tests. Two additional branches for the Maxwell model were consequently necessary to describe the viscous response of the material. From a set of initial parameters $(c_1, c_2, c_3, \tau_1, \beta_1, \tau_2, \beta_2, \tau_3, \beta_3, \tau_4, \beta_4)$, in which $\tau_1 = 8.4$ s and $\tau_2 = 16$ s (results from previous sections), stress-stretch curves were computed from finite element computations. The parameters were adjusted using the least squares technique associated to Levenberg-Marquardt scheme to ensure that the curves fit the experimental nominal stress versus stretch curves. The result of the optimization procedure is presented in **Table 2**. It was obtained with a coefficient of determination $R^2 = 0.87$ for indentation/relaxation and $R^2 = 0.79$ for stress-free relaxation.

Table 2: Hyper-viscoelastic parameters of silicone: optimized set of values from MI test. The values of the relaxation times are reordered in ascending order

Parameters	c_1 (Pa)	c_2 (Pa)	c_3 (Pa)	$\beta_1, \beta_2, \beta_3, \beta_4$ (-)	$\tau_1, \tau_2, \tau_3, \tau_4$ (s)
Optimized values	3140	349	209	0.8, 0.04, 0.03, 0.2	1, 8.4, 16, 50

The corresponding evolutions of stress and displacement with time are shown in **Figure 6** (top). Optimized parameters enable the model to match the experimental data regarding indentation and relaxation stages. Concerning the stress-free relaxation stage, the model does not capture the instantaneous stress-free relaxation displacement but is consistent with the overall observed behavior. Within the range of loads imposed during these tests, the error in displacement measurement was estimated to be less than 1%.

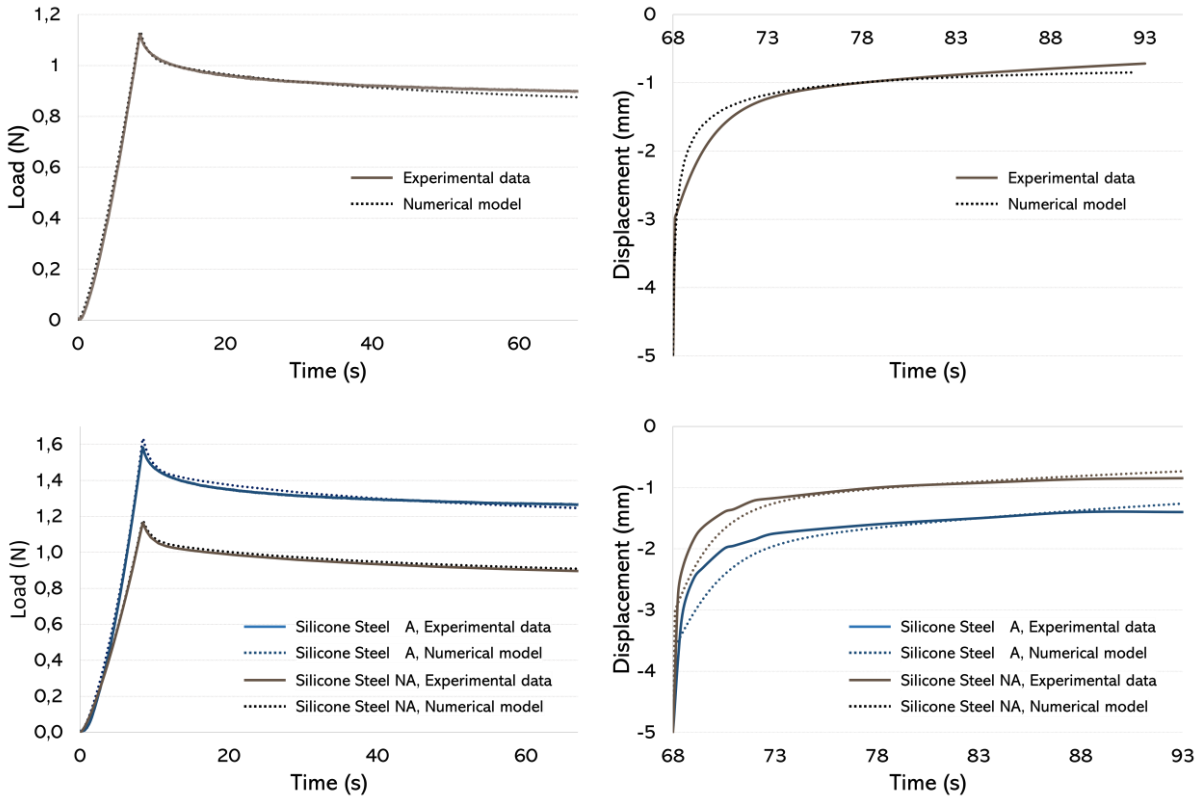

Figure 6: Comparison of the numerical (solid line) and experimental (dashed line) results for (left) the measured force during indentation and relaxation and (right) the displacement of the top surface during stress-free relaxation. Top figures correspond to silicone sample and bottom ones to silicon samples with adhesive (Silicone Steel A) and decohesive (Silicone Steel NA) inclusions.

Experimental validation on silicone samples with inclusions

The results of the simulations are analogously compared to those obtained from the experiments in the case of silicone with adhesive and decohesive inclusions. **Figure 6** (bottom) shows the numerical and experimental data in both cases. The numerical model reproduced well the load evolution for the indentation and relaxation stages ($R^2 = 0.88$). The evolution of the displacement is also in satisfying agreement with the experiments, especially the final position of the top surface, which will be one of the investigated parameters in the sensitivity analysis conducted further. Thus, the confrontation between experiments and modeling confirmed the validity of the numerical model for this study.

3. Results

3.1. Detection and characterization of a nodule via MI

The finite element model, introduced in the previous section, was used to investigate the possibility of detecting an inclusion inside a silicone sample, and to conclude on the nature of its adhesion (i.e. cohesive or decohesive) to the surrounding silicone. The evolution of load and displacement with time in the case of a silicone sample without inclusion and with an adhesive or non-adhesive inclusion are compared in **Figure 7** for an inclusion located at $(r, z) = (0, 1.6\ \text{cm})$.

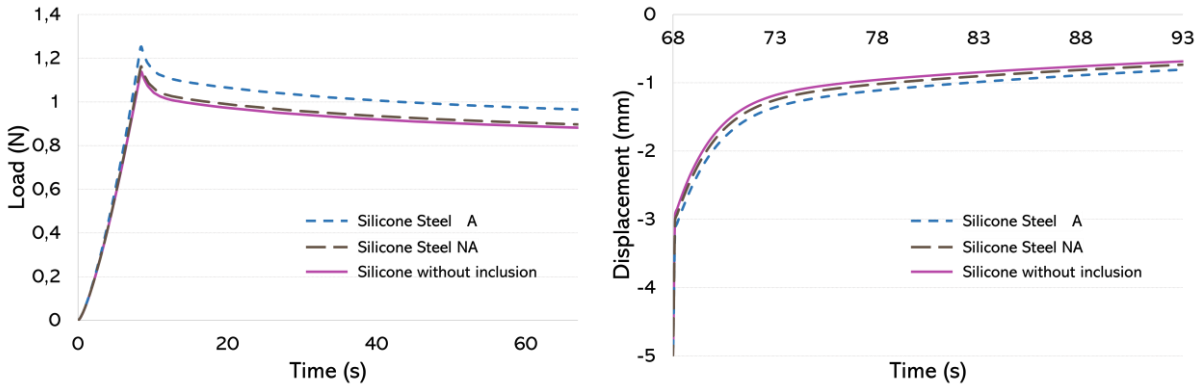

Figure 7: Predictive simulations of the (left) indentation, relaxation and (right) stress-free relaxation phases for raw silicone, silicone with adhesive inclusion and silicone with non-adhesive inclusion. The inclusion is located at (r,z)=(0,1.6 cm).

The values of the indicators introduced in the previous section, F_M, F_m and d_M, are listed in **Table 3** for the silicone with and without inclusions (adhesive or not) with the associated variation compared to the silicone sample without inclusion. These results show that the presence of an adhesive inclusion yields an increase of F_M and F_m by approximately 10 % and of d_M by 12.5 %. In the case of a non-adhesive inclusion, this increase is around 2 % only. Hence, for this specific size, position of inclusion and imposed indentation depth, the instrumented indentation would not enable the detection of inclusions with sliding interface, due to the non-significant difference between the measures of the silicone without inclusion and that with a non-adhesive inclusion. The results are nevertheless encouraging for the detection of adhesive inclusions, whose response to MI is more significantly different from that of silicone without inclusion than silicone with a non-adhesive inclusion. The reason of the influence of the nature of the adhesion between the inclusion and the surrounding silicone on the response of the material to MI is investigated in the next section.

Table 3: Values of curves indicators for raw silicone, silicone with adhesive and non-adhesive inclusions.

	Indentation F_M (N)	**Relaxation** F_m (N)	**Stress-free relaxation** d_M (mm)
Silicone	1.14	0.87	-0.72
Silicone Steel A	1.25	0.96	-0.81
Variation compared to raw silicone	**9.65**	**10.34**	**12.50**
Silicone Steel NA	1.16	0.89	-0.73
Variation compared to raw silicone	**1.75**	**2.30**	**1.39**

Furthermore, the sensitivity of the stress-free relaxation phase, measured through d_M, is also encouraging. Indeed, the stress-free relaxation distance d_M can be normalized by the indentation depth, which can be known when performing the measure. Hence, its value is more likely to be independent of the operator, i.e. the physician who perform the exam on the patient, which contributes to having a more quantitative than qualitative appreciation of the potential malignancy of the tumor.

3.2. Influence of the nature of the adhesion of the inclusion of the stress field

The effect of the nature of an inclusion, located at $z = 2.3$ cm, on the von Mises stress is illustrated in **Figure 8**. In the case of an adhesive inclusion, the initial stress concentration is located just below the indenter. This position is shifted to a location within the silicone at the end of the indentation stage (see Figure *8*a). At the end of the stress-free relaxation stage, this maximum is shifted to lower values. In the case of the sliding interface, a tangential displacement occurs at the interface, leading to a global stress decrease. This phenomenon explains the reduction of the indicators observed in the case of non-adhesive inclusions, highlighted in the previous section.

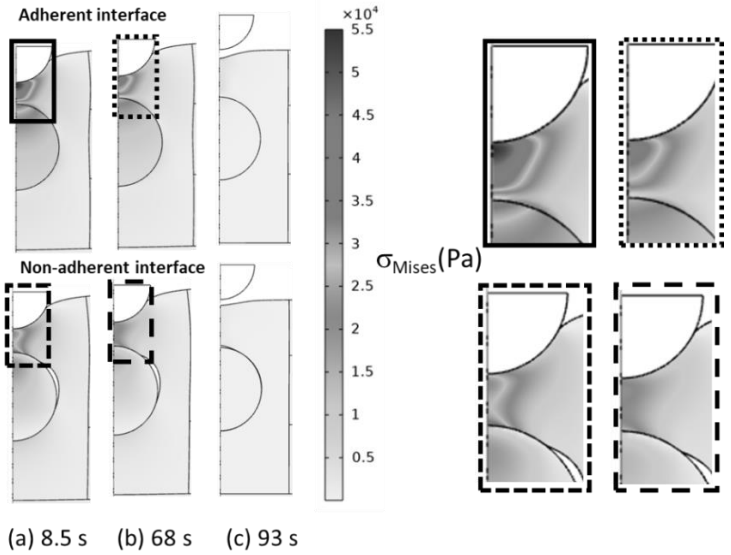

Figure 8: Von Mises stress field for (top) adherent and (bottom) non-adherent inclusion in silicone at different relaxation times, corresponding to the three phases: (a) indentation, (b) relaxation and (c) stress-free relaxation. The center of the inclusion is located at $z = 2.3$ cm. Inset on the right are zoomed parts of the fields.

The value of the von Mises stress reached inside the silicone sample seems to depend on the distance between the indenter and the inclusion. A sensitivity analysis is therefore conducted in the next section in order to quantify the dependence of the indicators F_M, F_m and d_M to the size and position of the inclusion.

3.3. Sensitivity of the MI measure to the size and position of the inclusion

The effect of the size and vertical position of centered inclusions ($r = 0$) on the measure of F_M, F_m and d_M, is investigated. First, the variation of these variables, in terms of the radius of the nodule, is represented in **Figure 9**a, for a nodule located at $z = 18$ mm (in the center of the silicone sample). The radius of the inclusion is varied between 8 and 16 mm. It is worth recalling that the results presented earlier in the manuscript have been obtained for an inclusion whose diameter is 12 mm, and that the height of the silicone sample is 36 mm. For small inclusions (less than 8 mm in diameter), all indicators are similar (absolute variation compared to silicone without inclusion smaller than 5 %), which demonstrates that inclusions whose diameter is smaller than 8 mm cannot be detected, since the response to MI is the same, regardless of the presence and the nature of an inclusion. It also appears that non adhesive inclusions are more likely to be detected if their diameter is large (variation compared to silicone without inclusion close to 10 % for inclusions of diameter 16 mm). The influence of the size of the inclusion on

the MI indicators is nonetheless much larger for adhesive than for non-adhesive inclusions: the larger the inclusion, the more likely it is to be detected.
A second sensitivity analysis is subsequently conducted in order to investigate the influence of the vertical position z of an inclusion of diameter 12 mm on its detection via MI, depending on the nature of its adhesion to the silicone. The position of the inclusion is varied between 15 mm and 21 mm, recalling that $z = 18$ mm is the centered position and $z = 36$ mm is the position of the top surface of the sample. Figure 9b depicts the effect of z on the variation of F_M, F_m and d_M, in the case of adhesive and non-adhesive inclusions, compared to raw silicone. The closer the inclusion from the top surface, the easier it is to detect it.

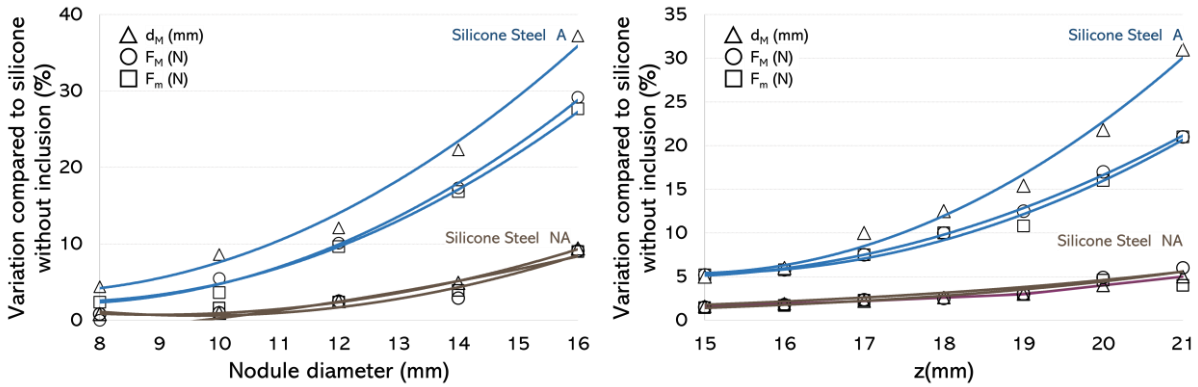

Figure 9: Absolute variation of F_M, F_m and d_M, compared to measures on silicone samples without inclusion, in terms of (left) the diameter of an inclusion location at $(r, z) = (0, 18)$ mm and (right) the z position of a centered inclusion $(r = 0)$ of diameter 12 mm. The solid lines are trend curves.

None of the indicators seems to be prominent to identify non-adhesive inclusions regardless of their size and position, since their sensitivity to these parameters is the same. Furthermore, their variations compared to the measure for raw silicone do not exceed 6 %, except for large inclusions (16 mm in diameter, i.e. almost half the thickness of the sample). The use of these measures for the identification of non-adhesive inclusions can therefore not be validated.
The results of this sensitivity analysis tend to show that the MI device does not provide sufficiently discriminant indicators to identify non-adhesive tumors in a breast tissue, as the response of the tissue with or without the non-adhesive tumor is similar. The device is however promising for the detection of adhesive tumors, as long as they are not too small (at least 12 mm in diameter) or too far from the skin (less than 19 mm under the surface). Furthermore, the stress-free relaxation phase, measured via d_M, which varies more than F_M and F_m when an adhesive inclusion is detected. Since the adhesiveness of a tumor can, in some cases, be an indicator of its malignancy, this result is very encouraging for the future applications of the monitored indentation device, that may enable to obtain a quantitative and independent-of-the-operator indicator of the presence of a malignant tumor within the breast tissue of a patient.

Conclusion

The objective of the present article was to investigate the feasibility of detecting inclusion in elastomer matrix via indentation and to enhance the interest of coupling this test with two supplementary stages: relaxation and stress-free relaxation, the latter stage being less operator dependent than the former. The main conclusion is that indentation enables the detection of an adhesive inclusion as far as it is large enough and close to the top surface. The stress-free

relaxation stage is even more sensitive to the presence of inclusion in comparison to the indentation stage and has the advantage to be less operator dependent. Non adherent inclusion cannot be detected by indentation test even in the stress-free relaxation stage. This conclusion is for an inclusion which is aligned with the indenter, an offset indentation would lead to shearing more and hence to enhance discrepancies. This preliminary study must be completed with deformable and misaligned inclusions of different shapes, with various tests conditions (speed, contact, relaxation times) and by integrating uncertainties due to the operator. Furthermore, the results presented in this article were obtained using a model of perfect shape of steel inclusions in a silicone sample. These two materials have a larger discrepancy in stiffness than biological materials would have. It is therefore necessary to be careful with these results and to verify their applicability for such material.

Acknowledgements

The authors would like to thank Claire Longuet (IMT Mines Alès) for silicone formulations and Belkacem Otazaghine (IMT Mines Alès) for technical support in chemistry.

The authors have no conflict of interest to declare.

References

Avril, S., M. Bonnet, A. S. Bretelle, M. Grédiac, F. Hild, P. Ienny, F. Latourte, D. Lemosse, S. Pagano, E. Pagnacco, and F. Pierron. 2008. “Overview of Identification Methods of Mechanical Parameters Based on Full-Field Measurements.” *Experimental Mechanics* 48(4). doi: 10.1007/s11340-008-9148-y.

B., Alekya, Sanjay Rao, and Hardik J. Pandya. 2019. “Engineering Approaches for Characterizing Soft Tissue Mechanical Properties: A Review.” *Clinical Biomechanics* 69(December 2018):127–40. doi: 10.1016/j.clinbiomech.2019.07.016.

Alliliche, W., Renaud, C., Cros, J. M., & Feng, Z. Q. (2023). Numerical simulation of mechanical tests on a living skin using anisotropic hyperelastic law. Journal of the mechanical behavior of biomedical materials, 141, 105755.

Bendtsen, L., Jensen, R., Jensen, N., & Olesen, J. (1995). Pressure-controlled palpation: a new technique which increases the reliability of manual palpation. *Cephalalgia*, *15*(3), 205-210.

Caro-Bretelle, A. S., P. Ienny, and R. Leger. 2013. “Constitutive Modeling of a SEBS Cast-Calender: Large Strain, Compressibility and Anisotropic Damage Induced by the Process.” *Polymer (United Kingdom)* 54(17). doi: 10.1016/j.polymer.2013.06.006.

Chen, Zhaoyu, Tobias Scheffer, Henning Seibert, and Stefan Diebels. 2013. “Macroindentation of a Soft Polymer: Identification of Hyperelasticity and Validation by Uni/Biaxial Tensile Tests.” *Mechanics of Materials* 64:111–27. doi: 10.1016/j.mechmat.2013.05.003.

Deuschle, Julia K., Gerhard Buerki, H. Matthias Deuschle, Susan Enders, Johann Michler, and Eduard Arzt. 2008. “In Situ Indentation Testing of Elastomers.” *Acta Materialia* 56(16):4390–4401. doi: 10.1016/j.actamat.2008.05.003.

Giannakopoulos, A. E., and A. Triantafyllou. 2007. “Spherical Indentation of Incompresssible Rubber like Materials.” *Journal of the Mechanics and Phsysics of Solids* 55:1196–1211.

Haddad, S. M. H., S. S. Dhaliwal, B. W. Rotenberg, H. M. Ladak, and A. Samani. 2020. “Estimation of the Hyperelastic Parameters of Fresh Human Oropharyngeal Soft Tissues Using Indentation Testing.” *Journal of the Mechanical Behavior of Biomedical Materials* 108:103798.

Kalyanam, Sureshkumar, Kathleen S. Toohey, and Michael F. Insana. 2021. “Modeling Biphasic Hydrogels under Spherical Indentation: Application to Soft Tissues.” *Mechanics of Materials* 161(March). doi: 10.1016/j.mechmat.2021.103987.

Kuhl, C. K. 2000. “MRI of Breast Tumors.” *European Radiology* 10(1):46–58. doi: 10.1007/s003300050006.

Liao, Zisheng, Mokarram Hossain, and Xiaohu Yao. 2020. “Ecoflex Polymer of Different Shore Hardnesses: Experimental Investigations and Constitutive Modeling.” *Mechanics of Materials* 144:103366. doi: https://doi.org/10.1016/j.mechmat.2020.103366.

Liao, Zisheng, Jie Yang, Mokarram Hossain, Gregory Chagnon, Lin Jing, and Xiaohu Yao. 2021. “On the Stress Recovery Behavior of Ecoflex Silicone Rubbers.” *International Journal of Mechanical Sciences* 206(June):106624. doi: 10.1016/j.ijmecsci.2021.106624.

Moghaddama, A. O., J. Wei, J. Kim, A. C. Dunn, and A. J. Wagoner Johnson. 2020. “An Indentation-Based Approach to Determine the Elastic Constants of Soft Anisotropic Tissues.” *Journal of the Mechanical Behavior of Biomedical Materials* 103:103539.

McDonald, S., Saslow, D., & Alciati, M. H. (2004). Performance and reporting of clinical breast examination: a review of the literature. *CA: a cancer journal for clinicians*, *54*(6), 345-361.

Pierrat, B., D. B. MacManus, J. G. Murphy, and M. D. Gilchrist. 2018. “Indentation of Heterogeneous Soft Tissue: Local Constitutive Parameter Mapping Using an Inverse Method and an Automated Rig.” *Journal of the Mechanical Behavior of Biomedical Materials* 78(April 2017):515–28. doi: 10.1016/j.jmbbm.2017.03.033.

Rauchs, G., J. Bardon, and D. Georges. 2010. “Identification of the Material Parameters of a Viscous Hyperelastic Constitutive Law from Spherical Indentation Tests of Rubber and Validation by Tensile Tests.” *Mechanics of Materials* 42(11):961–73. doi: 10.1016/j.mechmat.2010.08.003.

Sparks, Jessica L., Nicholas A. Vavalle, Krysten E. Kasting, Benjamin Long, Martin L. Tanaka, Phillip A. Sanger, Karen Schnell, and Teresa A. Conner-Kerr. 2015. *Use of Silicone Materials to Simulate Tissue Biomechanics as Related to Deep Tissue Injury*.

Steinmann, P., H. Mokarram, and G. Possart. 2012. “Hyperelastic Models for Rubber-like Materials: Consistent Tangent Operators and Suitability for Treloar’s Data.” *Archive of Applied Mechanics* 82:1183–1217.

Yeoh, O. H. 1990. “Characterization of Elastic Properties of Carbon-Black-Filled Rubber Vulcanizates.” *Rubber Chem. Technol.* 63:792–805.

Zheng, Y., Crosby, A. J., & Cai, S. (2017). Indentation of a stretched elastomer. *Journal of the Mechanics and Physics of Solids*, 145-159.

ToC figure *((Please choose one size: 55 mm broad × 50 mm high or 110 mm broad × 20 mm high. Please do not use any other dimensions))*